Turkish Journal of Physics

http://journals.tubitak.gov.tr/physics/

Research Article

Turk J Phys
(2019) 43: 541 – 550
© TÜBİTAK
doi:10.3906/fiz-1907-2

Quality control of silicon pixel wafers for the CMS Phase-1 pixel upgrade

Kamuran DİLSİZ[1,2,*], **Süleyman DURGUT**[2], **Kai Yİ**[2,3], **Leonard SPIEGEL**[4]
[1]Department of Physics, Faculty of Arts and Science, Bingöl University, Bingöl, Turkey
[2]Department of Physics and Astronomy, University of Iowa, Iowa City, IA, USA
[3]Department of Physics, Nanjing Normal University, Nanjing, P.R. China
[4]Fermi National Accelerator Laboratory, Batavia, IL, USA

Received: 02.07.2019 • **Accepted/Published Online:** 10.09.2019 • **Final Version:** 05.12.2019

Abstract: The CMS detector at the CERN Large Hadron Collider features as its innermost component a silicon pixel detector. The original pixel detector was completely replaced during the 2016–2017 winter technical stop. One of the goals of this Phase-1 Upgrade of the pixel detector was to replace the sensors in the original CMS forward pixel detector with new, unirradiated sensors. The new CMS forward pixel detector must survive an integrated luminosity of 300 fb^{-1} before being replaced again prior to the High-Luminosity LHC era. Just as in the original construction, the Phase-1 forward pixel sensors were made of n^{+}-in-n Diffusion Oxygenated Float Zone silicon. This note documents the quality spot-checking of the new sensors, comparing our results with those provided by the vendor. In general there was good agreement between the results.

Key words: LHC, CMS, silicon pixel detector, Phase-1 Upgrade

1. Introduction

The Compact Muon Solenoid (CMS) is one of two general purpose detectors located at the Large Hadron Collider (LHC) at CERN. The main purpose of the detector is to identify and measure the energy and momentum of particles [1]. With a 12,500-t weight, a length of 22 m, and a diameter of 15 m, the detector records events resulting from proton–proton collisions. The charged particles produced at the center of the detector are bent by a magnetic field of 3.8 T, which is produced by a superconducting solenoid with a length of 13 m and an inner diameter of 5.9 m. The main CMS subdetectors are the tracker, the electromagnetic calorimeter, the hadronic calorimeter, and the muon system [2].

The tracker has a cylindrical shape and uses silicon as the active medium. It consists of a pixel detector and a strip detector [1]. Before the Phase-1 upgrade, the pixel system of the CMS detector provided up to three precise hits per track, which allowed the identification of secondary vertices and the tagging of long-lived particles such as b quarks [3]. The pixel system is the detector closest to the beam pipe, with the innermost pixel barrel layer in the Phase-1 upgrade located at a radius of about 3 cm from the interaction point. Radiation damage associated with collisions steadily degrades the performance of the silicon sensors, especially those closest to the interaction region, and ultimately leads to the need to replace the sensors. One purpose of the Phase-1 upgrade was to replace the original pixel modules so that, with the possible exception of the innermost barrel layer, the new modules would not require replacement until the HL-LHC era.

*Correspondence: kdilsiz@bingol.edu.tr

This work is licensed under a Creative Commons Attribution 4.0 International License.

The installation of the new pixel detector [4] was completed in early 2017 after an extended year-end technical stop. Figure 1 shows the layout of the original and upgraded pixel detectors. The Phase-1 pixel detector has one more barrel layer and one additional forward disk per side compared to the original detector. In the original pixel detector, the forward system consisted of 18 million pixels corresponding to a $0.3\,\mathrm{m}^2$ active area, while the forward system in the upgraded pixel detector contains 45 million pixels corresponding to a $0.7\,\mathrm{m}^2$ active area. The original detector was designed to operate for 200 fb^{-1} with an instantaneous luminosity of $1\times10^{34}\mathrm{cm}^{-2}\mathrm{s}^{-1}$. During Run 2 in 2017, the instantaneous luminosity was increased to $2\times10^{34}\mathrm{cm}^{-2}\mathrm{s}^{-1}$; this would have led to readout inefficiencies because of the limited buffer sizes in the original pixel readout chips (ROCs). The upgraded pixel detector improves the tracking efficiency because of the additional layers and, more importantly, because of the larger buffers in the new, digital ROCs [5]. The upgraded pixel detector maintains or improves the performance at an increased instantaneous luminosity of $2\times10^{34}\mathrm{cm}^{-2}\mathrm{s}^{-1}$ and in addition allows operation up to an integrated luminosity of 300 fb^{-1} [6]. The number of forward pixel (FPix) modules in the new system, 672, is identical to the number in the original system, but the FPix module designs are quite different in terms of the size of the ROC arrays. The modules in the Phase-1 detector consist of $\mathrm{n}^+-\mathrm{in}-\mathrm{n}$ sensors (n^+ readout side, n bulk, p backside) having a size of 16.2 $\times$64.8 mm^2. Two rows of eight ROCs are bump-bonded to metalized pads on the n^+-side of each sensor, connecting 66,560 pixels per ROC where each pixel has a size of 150 $\times$100 $\mu\mathrm{m}^2$.

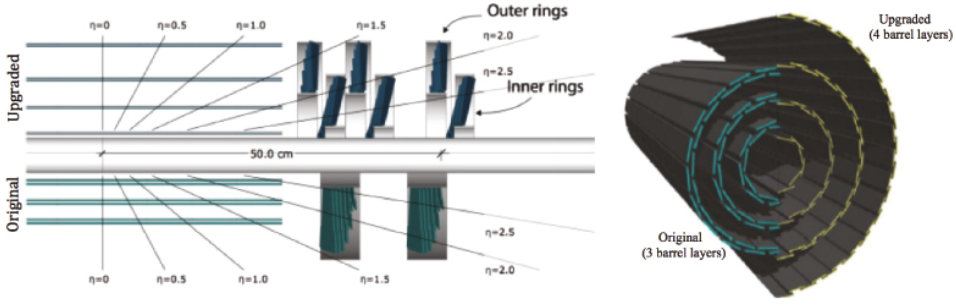

Figure 1. Layout of the original and the upgraded pixel detectors (left), and picture showing the layers of the original and upgraded pixel barrel detector (right) [4].

The Phase-1 FPix silicon sensors were fabricated and tested by Stiftelsen for Industriell og Teknisk Forskning [7] (SINTEF), a scientific and industrial research organization that has also fabricated the original FPix silicon sensors. In order to avoid bump-bonding of bad sensors to ROCs, the foundry tested all eight sensors on a wafer and provided detailed measurements of the current–voltage (IV) and capacitance–voltage (CV) characteristics for each batch of wafers. At the Fermi National Accelerator Laboratory (FNAL) a subset of the wafers was checked and the results were compared with the foundry results. If either the foundry data or FNAL data pointed to a problem with a particular sensor, the sensor was not used in the bump-bonding step. Contractually, the foundry could provide wafers with some bad sensors according to their measurement data provided that the overall yield exceeded an agreed upon threshold.

2. Production wafers and experimental test setup

A subset of the wafers delivered to FNAL were tested at the Silicon Detector center (SiDet) at FNAL. For each of the wafers that were tested, all eight sensors were probed. Figure 2 (left) shows the foundry sensor

numbering scheme as viewed from the p-side of the wafer. Included on the 150 mm diameter wafer are eight $2 \times 8\,\text{cm}^2$ sensors, six $1 \times 1\,\text{cm}^2$ sensors, four "slim-edge" sensors, and a number of diodes and other test structures (Figure 2, right).

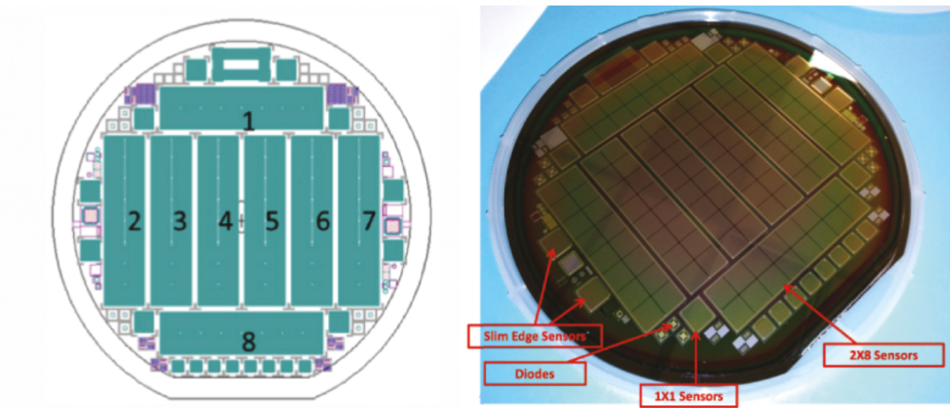

Figure 2. Drawing indicating the sensor numbering scheme (left) and photo of an actual wafer (right).

The FNAL wafer testing setup used a Summit 12000 AP probe station configured with two probe tips, a central-axis camera, and a movable chuck for supporting and fixing the wafer position. All of the testing was done at room temperature. The probe station chuck can be operated either through a PC keyboard or by a joystick, with the image of the wafer visible, under illumination, on the computer monitor. In order to measure the IV and CV curves, two ampere meters (Keithley 486 and Keithley 487) and an LCR meter (HP4784A) were used. Voltage was provided by a Keithley 237 source meter. Wafers were placed with the $n^{+}-$side down and in direct contact with the chuck. After the wafer was brought into position the chuck was raised slightly, thereby allowing contact with the two probe tips. The camera illumination was turned off prior to biasing. For the FNAL measurements we manually stepped the probe station chuck to allow measurements on all diodes and sensors. A rewiring was necessary to switch between IV and CV measuring modes.

3. Quality control of the production sensor wafers

The foundry produced 165 silicon wafers (1320 sensors) in total and shipped these to FNAL in five sets roughly corresponding to the production batches. Table 1 shows the reception dates and number of wafers in each delivery. As shown in the table, the foundry used letters to designate their production batches, where batch A (not included in the table) corresponded to a preproduction batch. For CMS database entries we used the following numerical convention:

- 9xx: A batch preproduction wafers
- 0xx: B batch production wafers
- 1xx: C batch production wafers
- 2xx: D batch production wafers
- 3xx: E batch production wafers,

where "xx" is the foundry designation.

To minimize damage to wafers during handling and to complete probing measurements in a reasonable period, 5–10 wafers per shipment were randomly selected. The IV and CV curves and breakdown voltages of all eight sensors on these selected wafers were measured. From the foundry data we understood the full depletion

Table 1. Naming convention and total number of delivered wafers.

Reception dates	B	C	D	E	Total
27 March 2015	21	-	-	-	21
29 May 2015	3	21	-	-	24
4 June 2015	5	33	-	-	38
27 October 2015	-	-	37	-	37
2 May 2016	-	-	-	45	45
Total	29	54	37	45	165

voltage for objects on the wafer to be around 65 V. To replicate the contractual acceptance criteria, we judged sensors to be good provided that (1) the total current at 100 V was less than 1 μA (1st criterion) and (2) the total current at 150 V was less than two times the current at 100 V (2nd criterion). Figure 3 shows the FNAL CV measurement of one 2 $\times$ 8 sensor and a diode on wafer 009, indicating the depletion voltage is about 65 V as expected. We did the same test on all randomly selected wafers and found that the depletion voltage was almost the same for all sensors [8]. In the following the IV results from the sample testing at FNAL and the comparison with the foundry "good" and "bad" determinations are described.

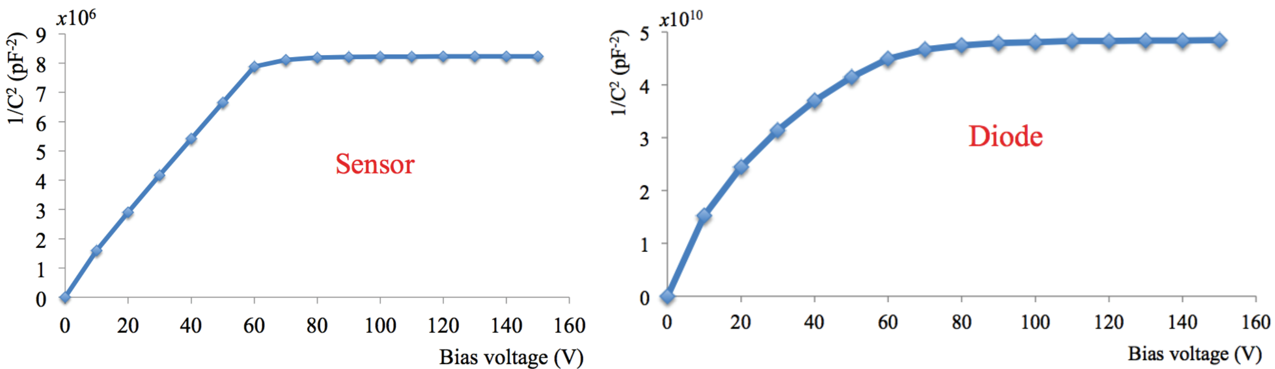

Figure 3. CV curves for a sensor (left) and a diode (right) on wafer 009.

Figure 4 shows the IV curves for the wafers with completely good sensors, from both the FNAL and foundry perspectives. As can be seen in the figure, both sets of data are within the acceptable ranges. Because of some differences in the two setups, such as the room temperature or the method with which the n^+−side of the wafer is in contact with the chuck, the measurements are not expected to be identical. There were a small number of sensors where there was a disagreement between the FNAL and foundry good/bad determinations. Sensors that are good according to the foundry data but bad according to FNAL data are shown in Figure 5. As can be seen in the figure, the IV curves for sensor 8 on wafers 009, 136, and 206 and sensors 3 and 4 on wafer 022 do not meet the second criterion. For these sensors, the total current is within the specification (1st criterion), but the slope is too high (2nd criterion). In addition, sensor 7 on wafer 324, sensor 6 on wafer 214, and sensor 8 on wafer 346 are not consistent with the first criterion. However, the foundry data for these sensors do not show any bad behavior. Figure 6 shows the sensors that were found good at FNAL but were labeled bad by the foundry. As shown in this figure, the foundry data for sensor 3 on wafer 028 and sensor 7 on wafer 022 are not consistent with the second criterion. All sensors for which an inconsistency between the FNAL and the foundry test was observed are listed in Table 2.

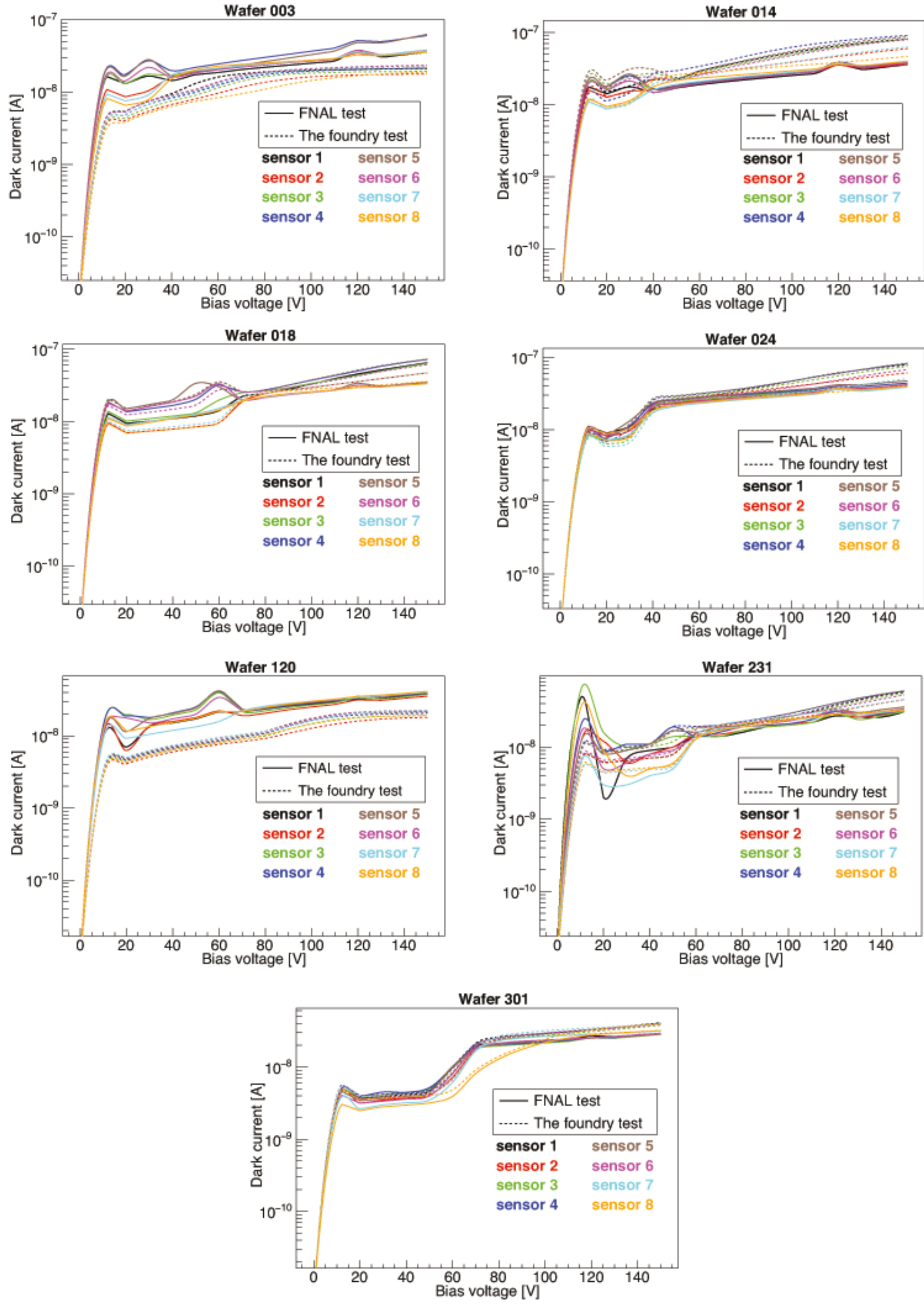

Figure 4. Wafers with all (8) good sensors.

The number of good and bad sensors from FNAL and the foundry tests are given in Table 3. According to FNAL (foundry) test results, there are 208 (215) good sensors out of 239 (240) probed sensors. In total, for the selected wafers, there are 10 sensors (4.2%) where there is a disagreement in the labeling of the sensor. Table 4 shows the number of wafers that have 8, 7, and 6 (or fewer) good sensors according to the foundry. From the full set of wafers (1320 sensors), the foundry found 1265 good sensors for a yield of 96%.

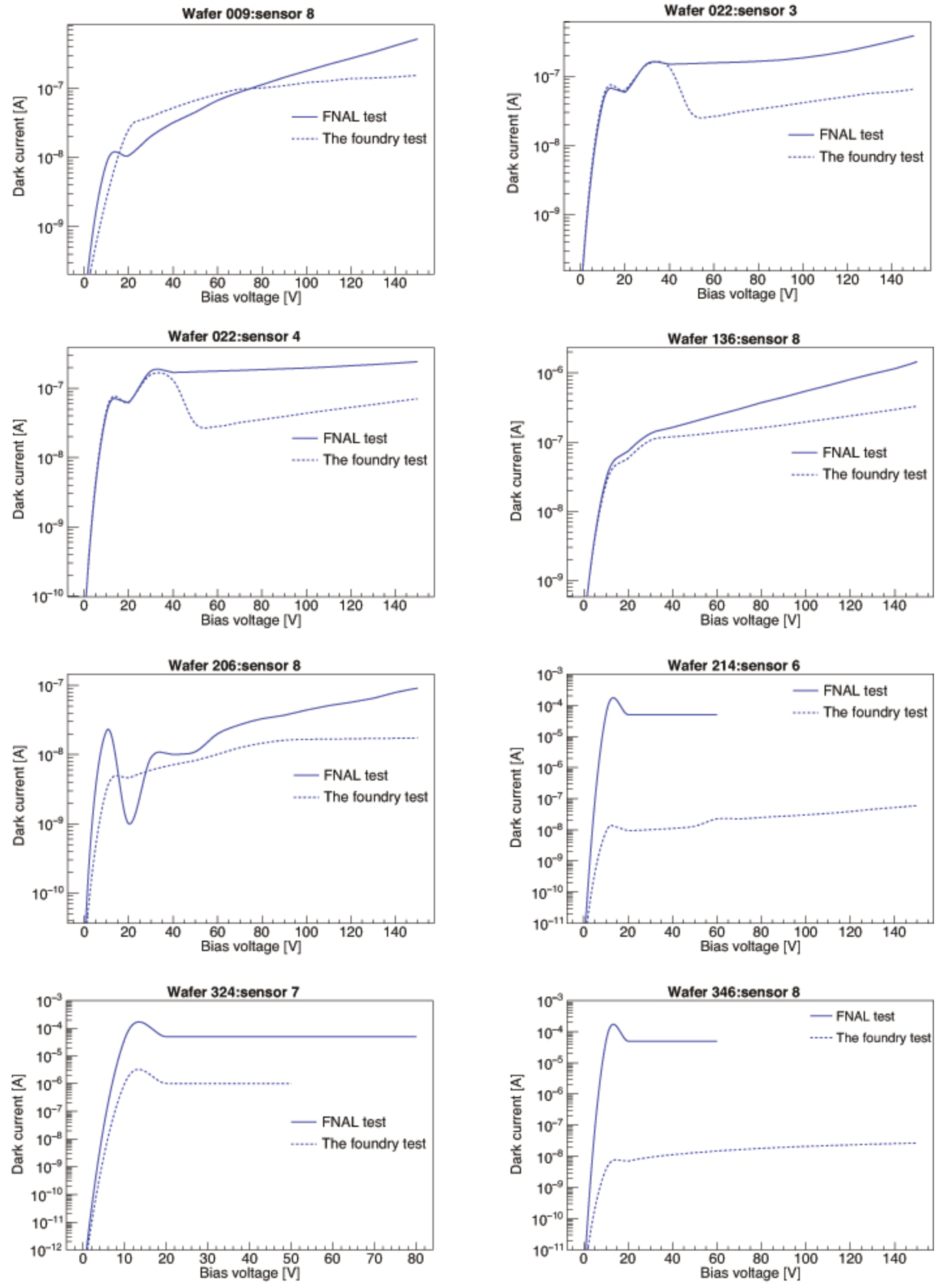

Figure 5. IV curves for sensors that were good according to the foundry's measurements but bad according to FNAL measurements.

4. Breakdown voltages

The "breakdown" voltages for all (8) sensors of the wafers given in Table 2 are shown in Figure 7. Both FNAL and the foundry continued the IV measurements beyond 150 V although this measurement was not part of the acceptance test. At the foundry, the voltage was increased until a current of $1\,\mu$A was reached. The FNAL measurements were instead performed with a current compliance of $50\,\mu$A. To directly compare with the foundry procedure the first values in the FNAL data where the current exceeded $1\,\mu$A were selected. Even

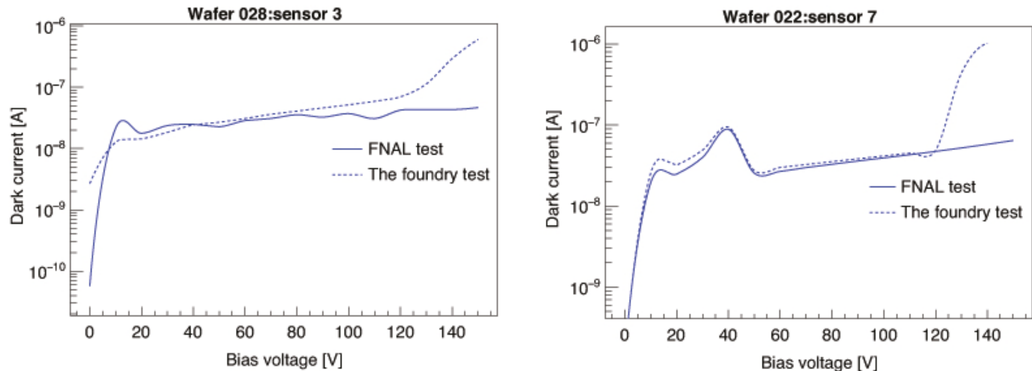

Figure 6. IV curves for sensors that were good according to FNAL measurements but bad according to the foundry's measurements.

Table 2. List of the sensors for which an inconsistency between the FNAL and the foundry test was observed.

Wafer	Bad by FNAL test but good by the foundry test		Bad by the foundry test but good by FNAL test	
	Sensor number	Criterion causing inconsistency	Sensor number	Criterion causing inconsistency
009	8	Second criterion	-	-
022	3 and 4	Second criterion	7	Second criterion
028	-	-	3	Second criterion
136	8	Second criterion	-	-
206	8	Second criterion	-	-
214	6	First criterion	-	-
324	7	First criterion	-	-
346	8	First criterion	-	-

with this adjustment the "breakdown" voltages at FNAL are consistently higher. However, as had been noted by the vendor, the sensor "breakdowns" are dominated by surface effects where some of the pixels do not receive bias from the chuck. The true breakdown voltages, as would be seen after bump-bonding or as inferred from the diodes on the wafers, are much higher than 600 V. One explanation for the difference in observed breakdown voltages may be the use of conductive rubber between the chuck and sensor in the foundry measurements. In order to assure the flatness of the wafers the sensor $n^{+}-$sides were in direct contact with the chuck at FNAL.

5. Summary

In this study, the quality of 239 sensors on 30 wafers from out of 165 wafers provided by the foundry was tested. Based on FNAL criteria for a sensor to be considered good, we found only 10 sensors where there was some disagreement between FNAL and the foundry probing results. Out of 239 sensors from the sampled wafers there were 229 sensors where the FNAL results agreed with the foundry's evaluation. The results showed that the consistency between FNAL and the foundry results is 95.8% (4.2% discrepancy). According to the foundry's own measurements, there were 1265 good sensors out of the 1320 sensors, corresponding to 96% yield. FNAL CV measurements of sensors and diodes indicate a 60–70 V full depletion voltage, which is close to the depletion voltage given by the foundry. In conclusion, the FNAL results confirmed the foundry results, which were good enough to assure that the sensors were appropriate for bump-bonding. All of the foundry results and the FNAL measurements have been uploaded to a CMS central database.

Table 3. The number of good and bad sensors by FNAL and the foundry criteria. According to FNAL criteria, there were 208 good sensors out of 239 sensors that were probed. According to the foundry, there were 215 good sensors out of 240 sensors for the same wafers.

Wafer no.	Number of good sensors		Number of bad sensors	
	FNAL data	Foundry data	FNAL data	Foundry data
002	7	7	1	1
003	8	8	0	0
006	7	7	1	1
009	7	8	1	0
010	6	6	2	2
014	8	8	0	0
016	7	7	1	1
018	8	8	0	0
020	6	6	2	2
022	5	6	3	2
024	8	8	0	0
028	8	7	0	1
106*	6	7	1	1
109	7	7	1	1
112	7	7	1	1
120	8	8	0	0
127	7	7	1	1
136	7	8	1	0
139	7	7	1	1
143	7	7	1	1
206	7	8	1	0
214	6	7	2	1
222	7	7	1	1
227	7	7	1	1
231	8	8	0	0
301	8	8	0	0
306	7	7	1	1
324	5	6	3	2
334	6	6	2	2
346	6	7	2	1
Total	208	215	31	25

*There are no FNAL data for sensor 8 on wafer 106.

Table 4. The number of wafers that have 8, 7, and 6 (or fewer) good sensors according to the foundry.

Batch	$N_{good}=8$	$N_{good}=7$	$N_{good}\leq 6$	Good sensors (%)
B	13	12	4	91
C	45	9	-	98
D	23	13	1	95
E	42	1	2	99
Total	123	35	7	96

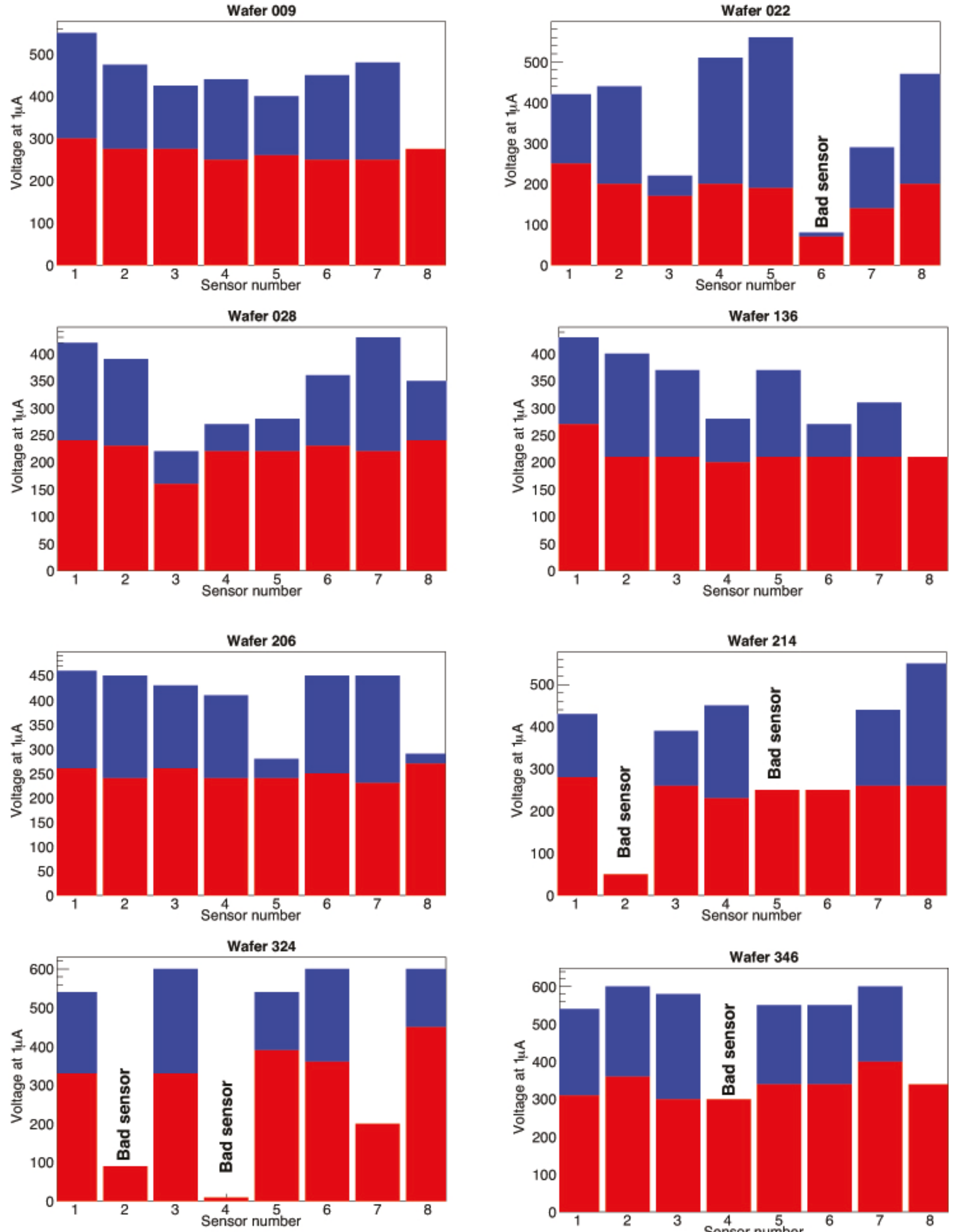

Figure 7. The voltages at which a current of $1\,\mu$A is reached for wafers 009, 022, 028, 136, 206, 214, 324, and 346. The blue (red) histograms show the data from FNAL (the foundry). The bar graphs are overlaid with the foundry entries in the foreground. Some of the FNAL entries are obscured but these are mostly for bad sensors.

Acknowledgment

This document was prepared in the framework of the CMS experiment using the resources of the Fermi National Accelerator Laboratory (FNAL), a US Department of Energy, Office of Science, HEP User Facility. FNAL is managed by Fermi Research Alliance, LLC (FRA), acting under Contract No. DE-AC02-07CH11359.

References

[1] CMS Collaboration. The CMS experiment at the CERN LHC. Journal of Instrumentation 2008; 3: S08004.

[2] CMS Collaboration. CMS Physics: technical design report. Volume I: Detector performance and software, CERN-LHCC-2006-001.

[3] CMS Collaboration. The Tracker Project Technical Design Report, CERN-LHCC- 98-06, CMS-TDR-5, 15 April 1998.

[4] CMS Collaboration. CMS Technical Design Report for the Pixel Detector Upgrade, CERN-LHCC-2012-016 (2012).

[5] Hits D, Starodumov A. The CMS pixel readout chip for the phase 1 upgrade. Journal of Instrumentation 2015; 10: C05029.

[6] CMS Collaboration. Technical Proposal for the Upgrade of the CMS detector through 2020, CERN-LHCC-2011-006, LHCC-P-004 (2011).

[7] The Foundation of Scientific and Industrial Research. https://www.sintef.no/en/

[8] Dilsiz K. Cross section measurement of simultaneously produced Υ (1S) + J/ψ mesons and upgrade studies for the CMS detector. PhD, University of Iowa, Iowa City, IA, USA, 2016.